Agency: U. S. Geological Survey
Award Number: 06HQGR0149 Project Title:

Holocene Seismicity of the Cascadia Subduction Zone Based on Precise Dating of the Turbidite Event Record

End Date: 09/30/2007

Final Technical Report

Principal Investigators:	Chris Goldfinger (PI) COAS Oregon State University 104 Ocean Admin Bldg. Corvallis, OR 97331-5503 (541) 737-5214 (541) 737-2064 (fax) email: gold@coas.oregonstate.edu
Authorized Institutional Representative	Peggy S. Lowry, Director of Sponsored Programs Oregon State University (541) 737-3437, (541) 737-3093 Fax sponsored.programs@orst.edu

Element Designation:	Elements I, II
Key Words	Turbidites, Paleoseismicity, Neotectonics, Seismotectonics

Abstract

This project continues our turbidite investigation along the Cascadia convergent margin, where submarine channels along the margin have recorded a Holocene history of turbidites mainly triggered by great earthquakes. Turbidite systems from Barclay canyon (Vancouver Island) to the Eel Canyon (Northern California), contain a remarkable record of turbidity currents triggered by great earthquakes during the Holocene, and pass several tests of synchronous triggering.

In the last two years we have found that event-specific signatures of each past event can be correlated between sites in Cascadia. These signatures are composed of density and high-resolution magnetic susceptibility, which in this context are proxies for grain size in the turbidites. We see multiple fining upward sequences stacked vertically within each turbidite, indicating multiple inputs closely spaced in time (within hours at a maximum). It is the pattern of these "pulses" that correlate in number, size, and vertical distribution, comprising a "signature" for each event that is easily recognizable at multiple sites. By correlating events using these unique signatures, supported by 14C ages, and ties to land paleoseismic data, we are beginning to see the spatial and temporal pattern of Holocene ruptures. Thus far, our results suggest that the turbidite record has recorded a total of 37 events. Initially 18 Holocene events were identified, now modified to 19 events, but newer cores off southern and central Oregon margin have improved the record there, and we now

recognize additional events that are isolated to southern Oregon and Northern California. Of these, we can correlate 19 events from at least the Rogue River to the Juan de Fuca Channel, comprising 70% of the margin. The additional events range from robust turbidites in the cores to thin mud turbidites that were originally not recognized as correlatable events, but are so now. These additional events can be correlated between sites, providing constraints on the northern and southern rupture limits in many but not all cases. The segmentation is compatible with onshore paleoseismic data also indicating margin segmentation of southern Cascadia.

The additional southern Cascadia events define a shorter recurrence interval for southern Oregon and Northern California and exists off the northern Cascadia margin, and an intermediate interval that applies to northern Oregon and southern Washington. The shorter interval for southern Oregon-Northern California is ~260 years, as comared with the northern interval of ~ 500 years. With 307 years since the last event in AD 1700, southern Cascadia has now exceeded the average repeat time for that region.

Investigations undertaken

Our tasks for FY 2006 included following:

- Use OxCal calibration software to improve timing constraints by integrating sedimentation rates and other known constraints with the offshore age model. Additional ^{14}C dates from backup cores will be acquired to fill holes in the time series. Models will also be constructed using the best available onshore data. Timing constraints will be improved through multi proxy approach to determine sedimentation rates and hemipelagic intervals between events.

- Improve correlations between events to determine the robustness of the stratigraphic record, and the limits of rupture.

- Complete a statistical analysis of site correlations to test their significance. This critical component is key to rupture length estimation from the turbidite record. OxCal models will be constructed both with and without these correlations.

- Compare results of spatial rupture distribution to structural models of Cascadia segmentation. While most Cascadia ruptures include most segments, energy release may be concentrated in these segments as is appears to be in other subduction zones.

We have been investigating the recurrence pattern of Great Earthquakes along the Cascadia margin using the record of turbidites deposited after margin-wide shaking during great earthquakes.

Concurrent with the discovery of the first buried marsh sequences on land, Adams, (1985; 1990) assessed the possibility that turbidites in channels of Cascadia Basin contained a record of great earthquakes along the Cascadia margin. He

examined core logs for the Cascadia Basin channels, and determined that many of them had between 13 and 19 turbidites overlying the Mazama ash datum. In particular, he found that three cores along the length of Cascadia channel contain 13 turbidites and argued that these 13 turbidites correlate along the channel (as did Griggs and Kulm, 1970). Adams observed that cores from Juan de Fuca Canyon, and below the confluence of Willapa, Grays, and Quinault Canyons, contain 14-16 turbidites above the Mazama ash. The correlative turbidites in Cascadia channel lie downstream of the confluence of these channels. If these events had been independently triggered events with more than a few hours separation in time, the channels below the confluence should contain from 26-31 turbidites, not 13 as observed. The importance of this simple observation is that it demonstrates synchronous triggering of turbidite events in channel tributaries, the headwaters of which are separated by 50-150 km. Similar inferences about regionally triggered synchronous turbidites in separate channels are reported in Pilkey (1988). The extra turbidites in the upstream channels may be the result of smaller events. This synchronicity test is a powerful relative dating technique that is completely independent of radiocarbon dating, which rarely has the precision to correlate events.

We have been using the turbidite record as a proxy for earthquake recurrence in both Cascadia and along the Northern San Andreas (Goldfinger et al, 2003a,b; 2005 in revision). Turbidite paleoseismology must of course demonstrate that the events recorded are earthquakes, and cannot always define the most recent events with the temporal precision of dendrochronology, however it is often more precise than trench dates, and extends much further back in time. In recent years, turbidite paleoseismolgy has been attempted in Cascadia (Adams, 1990; Goldfinger et al., 2003 a, b; Nelson et al., 1996; Nelson et al., 1999; Goldfinger and Nelson, 2000; Goldfinger et al., 2003), Puget Sound (Karlin and Abella, 1992), Japan (Inouchi et al., 1996; Shiki et al., 2000), the Mediterranean (Kastens, 1984; Nelson et al., 1995), the Dead Sea (Niemi and Ben-Avraham, 1994), northern California (Field et al., 1982; Field, 1984; Garfield et al., 1994) and even the Arctic ocean (Grantz et al., 1996), and is a technique that is evolving as a precise tool for seismotectonics.

In July, 1999, we collected 44 (4" diam.) piston cores, 44 companion trigger cores (also 4") and eight 30 cm box cores in every major canyon/channel system from the northern limit of the Cascadia subduction zone near the Nootka fault, to Cape Mendocino at its southern terminus (Figure 1; Goldfinger et al., 1999, 2003; Nelson and Goldfinger, 1999). Cores were run through the MST scanner as whole rounds to collect density, velocity, and magnetic susceptibility data, then split, photographed and described on board.

The investigation of recurring Great Earthquakes in Cascadia has led down several paths. Initially the story was told with marsh and tsunami data, and later the turbidite record is being used to extend and corroborate the land records. Like many pursuits, this investigation has branched in to several parallel paths that make up the framework of the project. At first we had three methods of looking at the event record: Relative dating techniques, radiocarbon results, and hemipelagic thickness between events. These three methods, though not totally independent (sedimentation rates depend on ^{14}C ages), offer a way to look at the record from different perspectives that should be compatible. Now, in

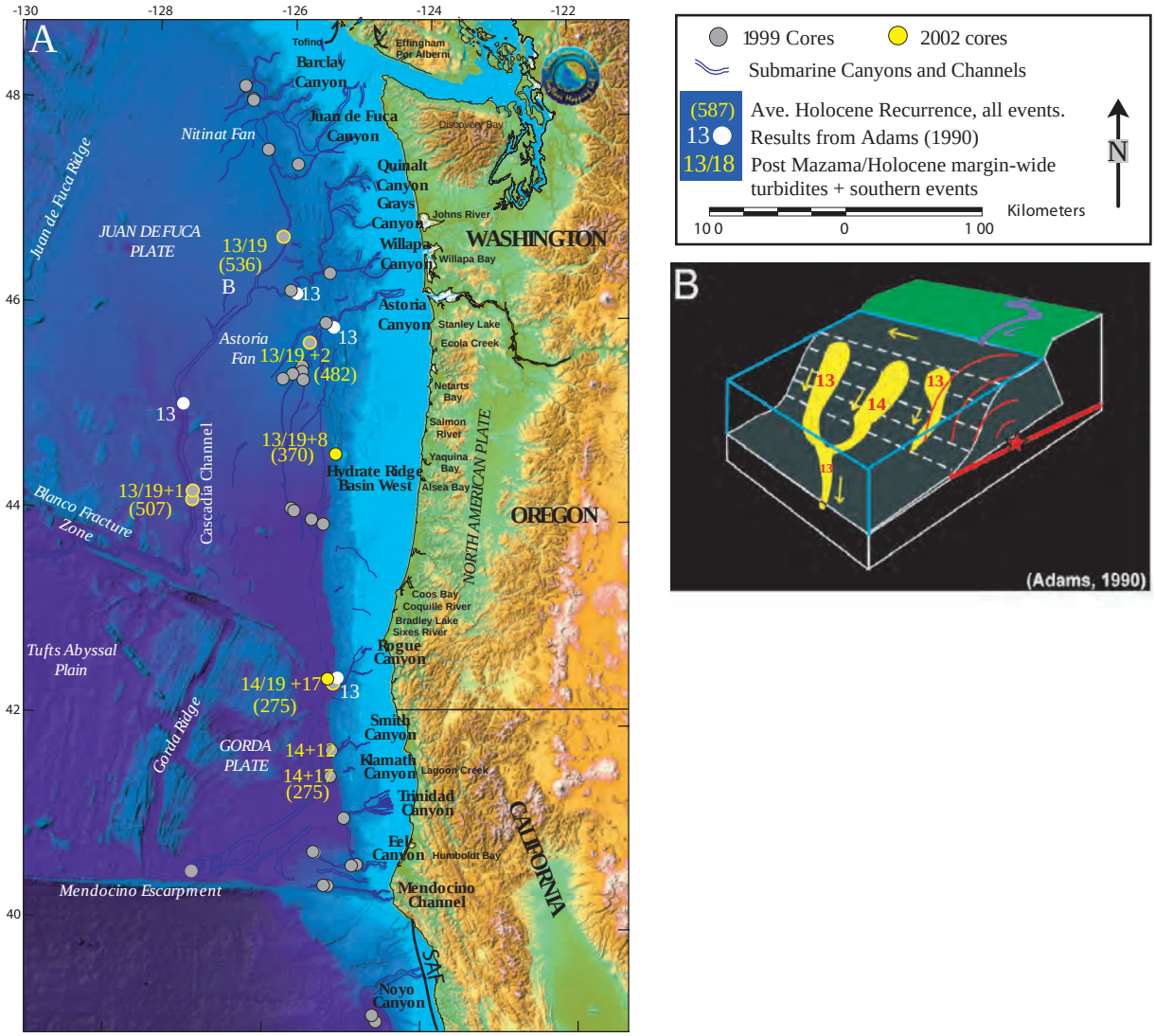
A
-130
-128
-126
-124
-122
48
46
44
42
40
Tofino
Effingham
Port Alberni
Barclay Canyon
Juan de Fuca Canyon
Discovery Bay
Nitinat Fan
Juan de Fuca Ridge
JUAN DE FUCA PLATE
Quinalt Canyon
Grays Canyon
Johns River
Willapa Canyon
Willapa Bay
WASHINGTON
13/19 (536)
B
13
Astoria Canyon
Stanley Lake
Ecola Creek
Astoria Fan
13/19 +2 (482)
Netarts Bay
Salmon River
Yaquina Bay
Alsea Bay
13/19+8 (370)
Hydrate Ridge Basin West
13/19+1 (507)
Cascadia Channel
Blanco Fracture Zone
OREGON
NORTH AMERICAN PLATE
Coos Bay
Coquille River
Bradley Lake
Sixes River
Tufts Abyssal Plain
Rogue Canyon
14/19 +17 (275)
Gorda Ridge
GORDA PLATE
14+12
14+17 (275)
Smith Canyon
Klamath Canyon
Lagoon Creek
Trinidad Canyon
Eel Canyon
Humboldt Bay
CALIFORNIA
Mendocino Escarpment
Mendocino Channel
SAF
Noyo Canyon
1999 Cores
2002 cores
Submarine Canyons and Channels
(587) Ave. Holocene Recurrence, all events.
13 Results from Adams (1990)
13/18 Post Mazama/Holocene margin-wide turbidites + southern events
N
100
0
100
Kilometers
B
13
14
13
13
(Adams, 1990)

Figure 1.

its mature stage, this investigation has yielded two new methods, pattern matching and direct physical property correlations that greatly strengthen the whole, and offer independent methods for assessing synchronous or asynchronous triggering of events along the margin. In the following section we discuss these methods and how they interrelate to form a robust framework. We here summarize recent results based on a multiple proxy approach to developing an age-event model for the Cascadia subduction zone. The multiple time-event proxies are:

1) Relative dating tools: Confluence tests, numerical event comparison.
2) AMS ^{14}C dating and age correlation
3) Hemipelagic thickness between events
4) Direct physical property correlation
5) Pattern matching between sites and between onshore and offshore records.

Our approach has been, and continues to be, to search for convergence of multiple approaches. Given the errors involved in each method, a common problem in paleoseismology, no single method can be relied upon solely to tell the story. Only a framework of multiple approaches that can be either complimentary or independent is likely to result in a coherent record.

The first three methods have been the staples of this project thus far. The last two are relatively new in this proposal. We discuss each of these methods and new results below.

Are the events all triggered by earthquakes? Other plausible triggers for turbidity currents include: 1) storm or tsunami wave loading; 2) sediment loading; 3) crustal and slab earthquakes; and 4) hyperpycnal flow. All of these mechanisms can trigger a turbidity current, but how can earthquake-triggered events be distinguished from other events? A fuller discussion can be found in Godfinger et al., (2003a,b). In our work, we primarily use spatial and temporal patterns of event correlations that cannot be the result of triggers *other* than earthquakes. Synchroneity of event records in separated canyons over wide region, and spanning a long time interval effectively eliminates most if not all non-earthquake triggers, which are usually limited spatially and temporally a to single canyon.

Only one other source, storm waves and hyperpycnal flow have potential to approximate a synchronous trigger over a large area. Hyperpycnal flow, or direct turbid injection from rivers, can produce turbid flows, and can even mimic earthquakes in that they may affect several rivers over a span of days. While this certainly occurred during Pleistocene lowered sea-level, when there was direct connection between rivers and offshore canyons, sea level-rise in the Holocene isolated most west coast canyons from the rivers. Sediment input now is distributed across the shelf and is not directly injected in the canyons (e.g. Sternberg, 1986, Wheatcroft et al. 2002). Tsunamis and storm waves may also conceivably act as a regional trigger. Our analysis shows that extreme storm waves that exist in the Pacific Northwest every winter have the potential to both erode and liquefy sediments at canyon head depths of ~ 120-150 m. However we see no evidence of such material reaching the abyssal plain, indeed there is nothing but hemipelagic sediment overlying the AD 1700 Cascadia earthquake. Puig et al. (2004) and other investigators have shown that this occurs, but also that such flows generally settle in the canyons in 200-500 m depth. Below this depth, the resuspended sediments are deposited. We note

that the tsunami from the 1964 Alaska Mw 9.0 event did not result in deposition of anything on the abyssal plain in our cores, although it did serious damage along the Pacific coast.

FY 2006 results

Direct Stratigraphic Correlation

In the course of investigating turbidites along the Cascadia and San Andreas margins using offshore cores, we have acquired continuous high resolution magnetic susceptibility, Gamma density, P-wave velocity, and loop magnetic data for all of the Cascadia cores. These profiles often are visually similar, as they reflect the underlying stratigraphic details in the cores. Physical property correlations are common practice with ODP cores, in the oil industry, and have recently come into use for paleoseismology (i.e. Abeldayem et al., 2003; St-Onge et al., 2003; Hagstrum et al., 2004, Iwaki et al., 2004; Karlin et al., 2004, Schnellmann et al., 2002). Turbidite "fingerprints" have been recognized and used for regional correlation in Lake Baikal (Lees et al., 1998), off Morocco (Wynn et al., 2002), and elsewhere.

Turbidite correlation is done using primarily magnetic susceptibility (MS) and density, much as e-logs are correlated in the oil industry (McCubbin et al.1992; Lovlie and van Veen, 1995). Physical property correlations of this type are also common practice with academic and ODP/IODP cores (e.g. (Fukuma, 1998) and have recently come into use for paleoseismology (i.e. (Karlin et al., 2004; Abdelayem et al., 2004; St-Onge et al., 2004; Hagstrum et al., 2004; Iwaki et al., 2004; Schnellman et al., 2002; Goldfinger et al., 2007a).

In addition to local site correlation, we have found that it is possible to correlate unique physical property signatures of individual turbidites from different sites within individual channels. This suggests that the processes controlling deposition of the turbidite maintain consistency for some considerable distance within a channel. We have also found it possible to correlate event signatures not only down individual channels and past confluences, but between channel systems separated by considerable distance, some of which never meet. These turbidite "fingerprints" form the basis of long-distance correlations, and are beginning to be recognized and used for regional correlation (e.g. Lake Baikal, Lees et al., 1998; off Morocco, Wynn et al., 2002; Cascadia, Goldfinger et al., 2003c; the Laptev Sea: Russian Arctic, Rivera et al., 2006, and elsewhere). Recently, the "event signatures" of Cascadia turbidites have been linked to coastal fjord records on Vancouver Island (Goldfinger et al., 2006b; Dallimore et al., 2005).

Typically, multi-pulse turbidites have only one fine tail (Bouma D) associated with waning of the turbidity current. The signatures we are correlating are comprised of these stacked coarse pulses. Goldfinger et al. (2007a) show in detail that the magnetic susceptibility, density, and grain size trends within each event are closely correlated. This is straightforward but important because we can in most cases use the high-resolution density and magnetic data as grain size proxies, at least for lithologies along the Cascadia and NSAF systems (Goldfinger et al., 2003c; Morey et al., 2003; Wynn and Masson, 2003). Further details of the use of magnetics and density as grain size proxies are given in Goldfinger et al., (2007a).

On close inspection of physical property logs, we sometimes see a remarkable similarity between correlative turbidites that are separated by as much as 500 km (Cascadia) and 280 km (NSAF). **Figure 2** shows several typical examples of correlative events over a distance of 470 km along the Cascadia margin. We see a general correspondence of relative turbidite thickness downcore that is reflected in separate channels, as well as correlable details such as the number of coarse sandy pulses (density and magnetic peaks). For example, Cascadia turbidite events T2, T10, and T12 are small events in all cores, whereas T11 and T16 are very large events in all cores, and many other events follow similar size patterns across both Cascadia and the NSAF margins. Vertical sequences of turbidite size and number of pulses are commonly preserved between remote sites, and were used to aid in the correlation framework. We observe similar patterns along the NSAF margin, where size trends, and individual characteristics persist over large distances. Goldfinger et al. (2007a) also show the evolution of a single event down channel over a distance of 74 km, showing the gradual merging of two sand pulses into a bimodal grain distribution. Stratigraphic correlation has the potential to establish links of individual events between core sites, independent of radiocarbon ages.

Figure 2 shows an example of stratigraphic correlation of several turbidites on the northern Cascadia margin, illustrating the details for two pairs of cores from three channel systems. Two classical approaches are commonly used in stratigraphic correlation. The simplest is visual, using corresponding remarkable features of both cores (e.g., Prell et al., 1986). Though its simplicity is appealing, this method may give subjective results, and may be somewhat arbitrary. The second method is to use a mathematical measure of the similarity between both signals--for example, a correlation coefficient--and then optimize this measure when adjusting the age-depth relation (Martinson et al., 1987). This procedure gives a more objective result, but the "fit" is not always as good as with the simple visual correlation, and the algorithms used are not nearly as powerful as those used by the human brain in pattern recognition. A mathematical measure such as a correlation coefficient will give more weight to the large timescale signal fluctuations (low-frequency variations) where much of the variance is located in the higher frequencies. With this method, the sharp events are not exactly in phase, as they should be according to the underlying simultaneity hypothesis. This second approach is, therefore, more objective, but often less precise. We use both approaches. With numerical correlations algorithms, one can place tie-points on one pair of signals, while interactively showing the effect on all other pairs. By changing pairs and adding and removing tie-points while controlling the result, it is possible to quickly establish a consistent, common stratigraphic scale. These analyses were used for site and regional correlations, as well as to define the tail/hemipelagic boundaries critical for timing constraints. **Figure 3** shows the most recent 3000 years of stratigraphic correlation, focusing on the southern Oregon margin using these techniques.

Radiocarbon Analysis

To date the turbidites, we extract planktic foraminifers from the hemipelagic sediment below each turbidite. We do this because the boundary between the top of the turbidite tail and the hemipelagic sediment is difficult to identify and bioturbation is concentrated at this boundary, possibly because the organic material brought down in the turbidite tail results in a benthic “bloom” (Smith et al, 1993). Sensitivity tests for species-specific biases are presented in Goldfinger et al. (2007a), as are the methods used to evaluate basal erosion. The close match

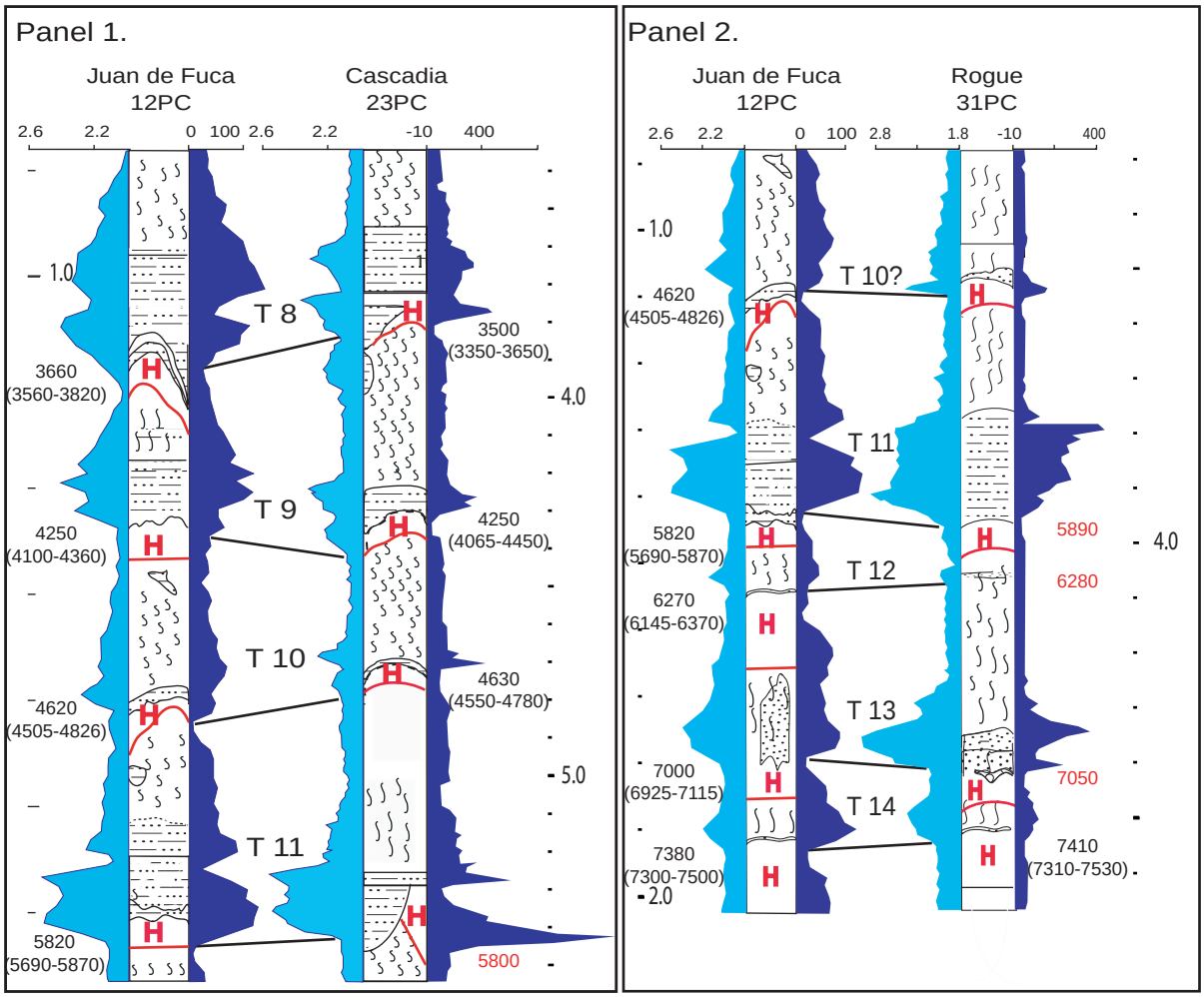

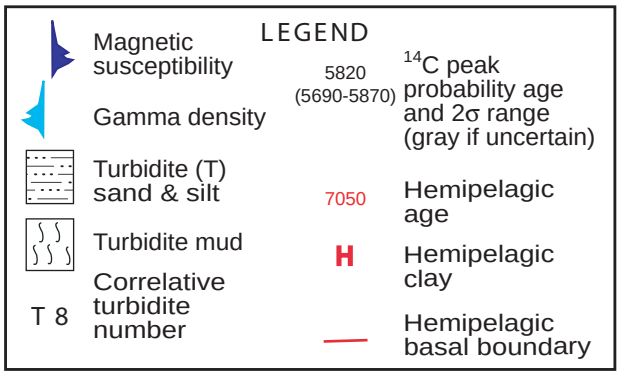

Figure 2: Correlation details from two pairs of cores on the Cascadia margin. Panel 1 shows events 8-11 in cores from Juan de Fuca Channel (left) and Cascadia Channel (right). Left traces are raw gamma density (light blue), right traces are magnetic susceptibility (dark blue). Lithologic logs are also shown. Note correspondence of size, spacing, number of peaks, trends between events, and "shape" of physical property traces between these cores. Panel two similarly displays events 10-14 in Juan de Fuca Channel (left) and Rogue Channel (right). Panel 1 cores are part of the same channel system, distance = 475 km. Panel 2 cores are in channels that do not meet, distance = 500 km.

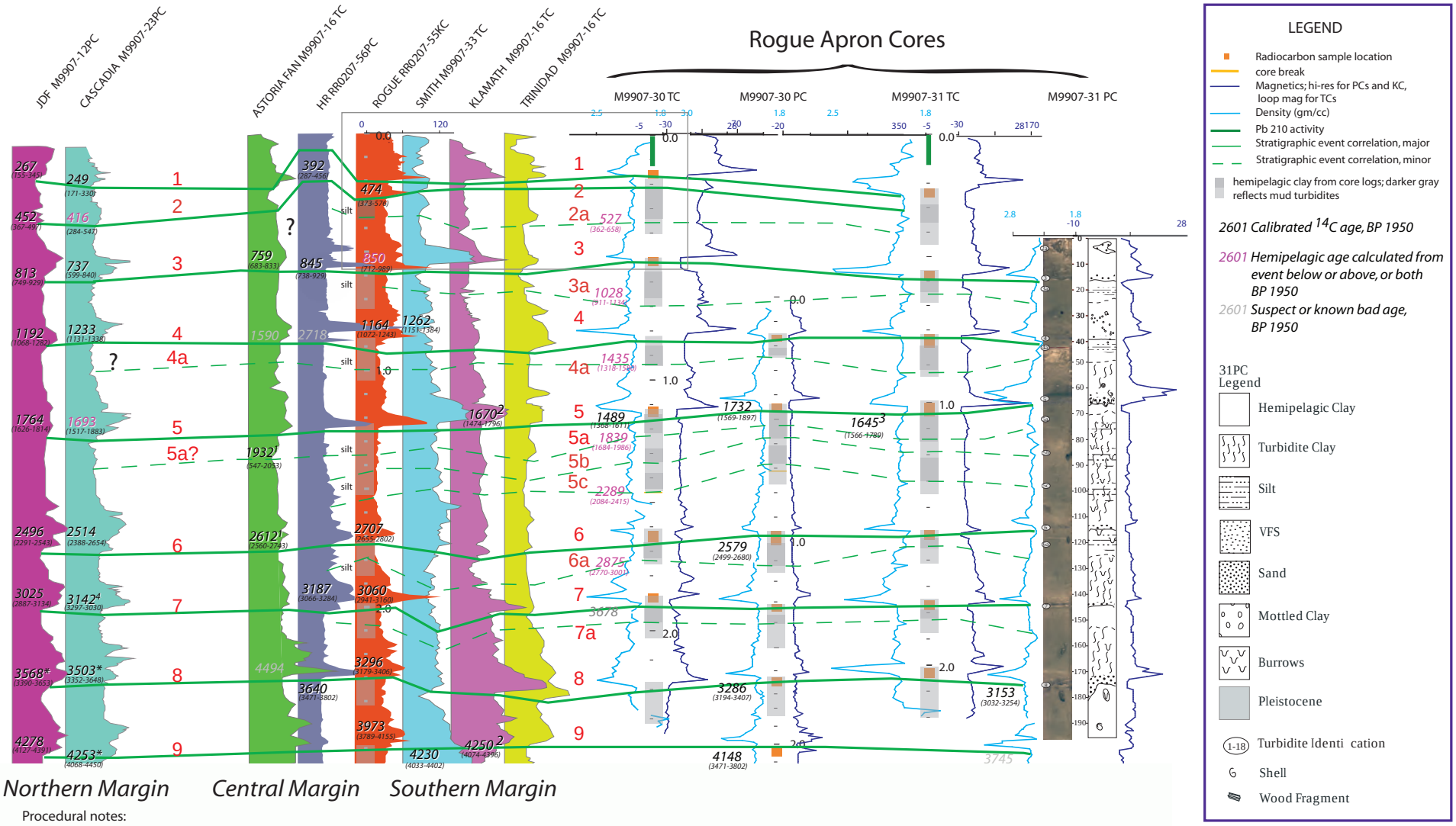

Procedural notes:

[1] These two ages were calculated from two samples that were not from the same event, they were mixed due to an original mis-correlation. Once the correlation was corrected, the age was calculated based on the average age of the two events that were mixed, adjusted for the weight ratio of forams inthe sample dated, if available, or by the ratio of sediment sample thickness if foram weights where sample wight was not available. We show this date only if it is in proper age progression, and agrees with other ages of the same correlated event. In this case, Astoria samples from T5A in 16PC, and T6 in 16TC. resulting age of 2260 is consistent with ages for T6 of 2612, and 1932 for T5a.

[2] As above, using ages based on age of sample 75 taken from T9 in 34PC, and T5 in 34TC. The resulting age of 3044 is consistent with ages for T5 of 1670, and 4250 for T9.

3 Mixed samples142 and 150 from T5 in 31PC, and above T5 in 31TC. The resulting age of 1647 is consistent with ages for T5. Log signatures suggest T4 H eroded, thus we assign this age as a minimum age for T5.

[4] As above, using ages based on age of sample 26 mixed from four subsamples from cores 22PC, 22TC, 23PC, and 23TC. Three of these were from T6, the fourth from T7. The resulting age of 2691 is consistent with mean ages for T6 of 2590, and 3142 for T7. using a proportion of 1:3 T7 to T6 sample by thickness.

* = Erosion correction applied see supplementary tables for calculation.

and lack of consistent bias in ages between land and marine events observed in both Cascadia and on the NSAF also suggests that neither bioturbation (Wheatcroft, 1992; Thomson et al., 1995) nor basal erosion significantly bias ^{14}C ages derived from planktic foraminifers in most cases.

Using a moving window average sedimentation rate, we corrected the original AMS ages for the radiocarbon sample thickness by subtracting the time corresponding to the thickness of the sample interval. Hemipelagic thickness was then converted to time for input into OxCal calibration software using the Marine04 database (Ramsey, 1995; Ramsey, 2001; Reimer et al., 2004). A sedimentation-rate regression analysis was employed to flag erosion at a given interval, and provide a check for consistency downcore, as sudden hemipelagic sedimentation rate changes in the marine environment are relatively rare. Outliers in this analysis are most likely caused by basal erosion because ages appear to be older, with less sediment thickness between events than expected. To evaluate flagged outliers, we tested them for basal erosion by comparing the hemipelagic thickness of that interval among several closely spaced cores. . In a few cases, multiple cores revealed that these anomalous intervals were the result of basal erosion on the core from which the sample was taken based on a thinner hemipelagic section in only that core. If the dated interval was found to wholly or partially come from an interval suspected of erosion, and other dating options were exhausted, we calculated a corrected age based on the full hemipelagic thickness represented in the nearby cores. We used a correction weighted in proportion to the sample weights, if more than one sample was used for the anomalous age. See Gutierrez-Pastor et al., 2007 for a full discussion of these methods. To verify this type of correction, or to calculate the age of an undated turbidite, we cane additionally calculate the age of the turbidite based on a dated turbidite below or above (or both if possible) the suspect/missing turbidite. The reference age above or below must be well dated at the suspect site and at other nearby sites to provide a stable reference. We can then calculate the age of the suspect event by adding the hemipelagic time to, or subtracting it from the reference age to establish a calculated age for the event. This can also be done with OxCal, though the Bayesian calculation actually provides weaker constraints than those of the analytical solution using the full hemipelagic time constraint. We have included ages corrected by these methods where the erosion correction and the calculated age methods produce similar results (significant overlap at the 1 sigma level). These are indicated as such the tables and figures, with calculations given in Table 2, electronic supplement.

Goldfinger et al.(2007a) illustrate use of OxCal to take advantage of multiple ages (if within analytical error of one another), including constraints imposed by the time represented by hemipelagic sediment between events. In one case (1700 AD event) we used historical information to restrict the age. Where age data are missing, sedimentation rates alone can be used to model event ages, which we have done for several events in our time series due to scarcity of foraminifers in those intervals. Goldfinger et al. (2008) show the analyses for the AD 1906 and the penultimate NSAF events (**Figure** 4), as well as the AD 1700 Cascadia event using OxCal with hemipelagic sedimentation and historical constraints. Using these well-known events, and time constraints provided by the hemipelagic sediment deposited in the interseismic period, OxCal returns the calendar age of the AD 1906 NSAF and AD 1700 Cascadia earthquakes to within a few years. The penultimate event is similarly constrained to a narrower time window than obtained by simple calibration. Further details of the OxCal analysis and the reservoir corrections applied are given in Goldfinger et al. (2007a). Also of importance here is the significance of the probability peaks in the PDF's. Multiple peaks and

broad distributions in the PDF's are generated largely from the slope of the atmospheric radiocarbon curves, and without other data, can only be treated statistically. For marine data in this study, we have both hemipelagic intervals that represent the time elapsed between turbidites, and sedimentation rate curves that serve to further constrain the time of emplacement.

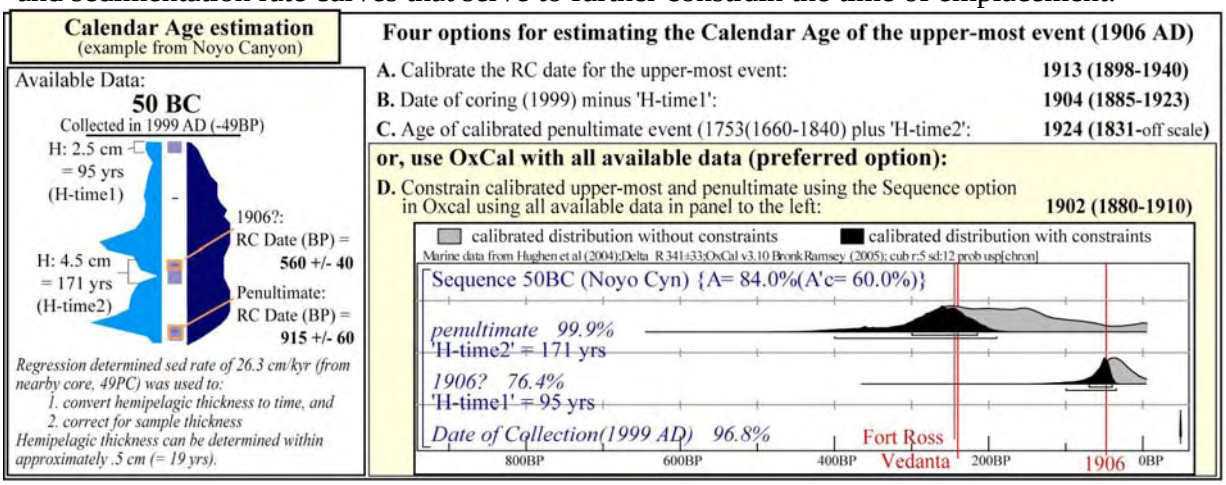

Figure 4. OxCal example (the very well constrained 1906 earthquake and associated paleoseismic data onshore and offshore are used here). The left panel shows the input data to OxCal, the raw radiocarbon ages and the hemipelagic thickness data, which is converted to time via sedimentation rate curves developed for each site. The right panel shows four ways to calculate the age for the 1906 earthquake, with the preferred method being the last, that is use of underlying and overlying hemipelagic intervals and 14C ages. The fort Ross and Vedanta mean ages for the penultimate event are shown, along with the OxCal solution for that event, calculated using the preferred method.

<u>Cascadia Time-Stratigraphic Event Correlation</u>

Figure 5 shows a space-time diagram for the Cascadia margin for the past ~ 3000 years including the land and marine data used in this study, as well as land data not included in the tabular age calculations. This figure shows the time series of major Cascadia margin events interpreted as earthquakes recorded both onshore and offshore. The onshore events have been subjected to rigorous tests of earthquake origin that typically comprise rapid subsidence and sudden burial of marsh surfaces with tsunami sand. Details of the tests applied to individual sites are contained in the original literature. We favor the most recent work in which these tests and sampling methods are more robust than in the earlier works, and favor sites that have multiple well-constrained ages for each event, and ages that use seeds, and needles over those that use peat plant material. Event records vary somewhat in their preservation of events, and in natural variability that comes from segmented margin ruptures. For events interpreted to be full margin events based on the joint land/marine data, we use the best ages from sites along the margin to constrain event ages. For southern Cascadia events, we follow Kelsey et al. 2005 and Nelson et al. (2006) in attempting to clarify segmented ruptures through addition of the marine turbidite record.

The total number of events in the 3000 year time range of this study, whether onshore or offshore, is similar, with a few differences noted below. The correspondence

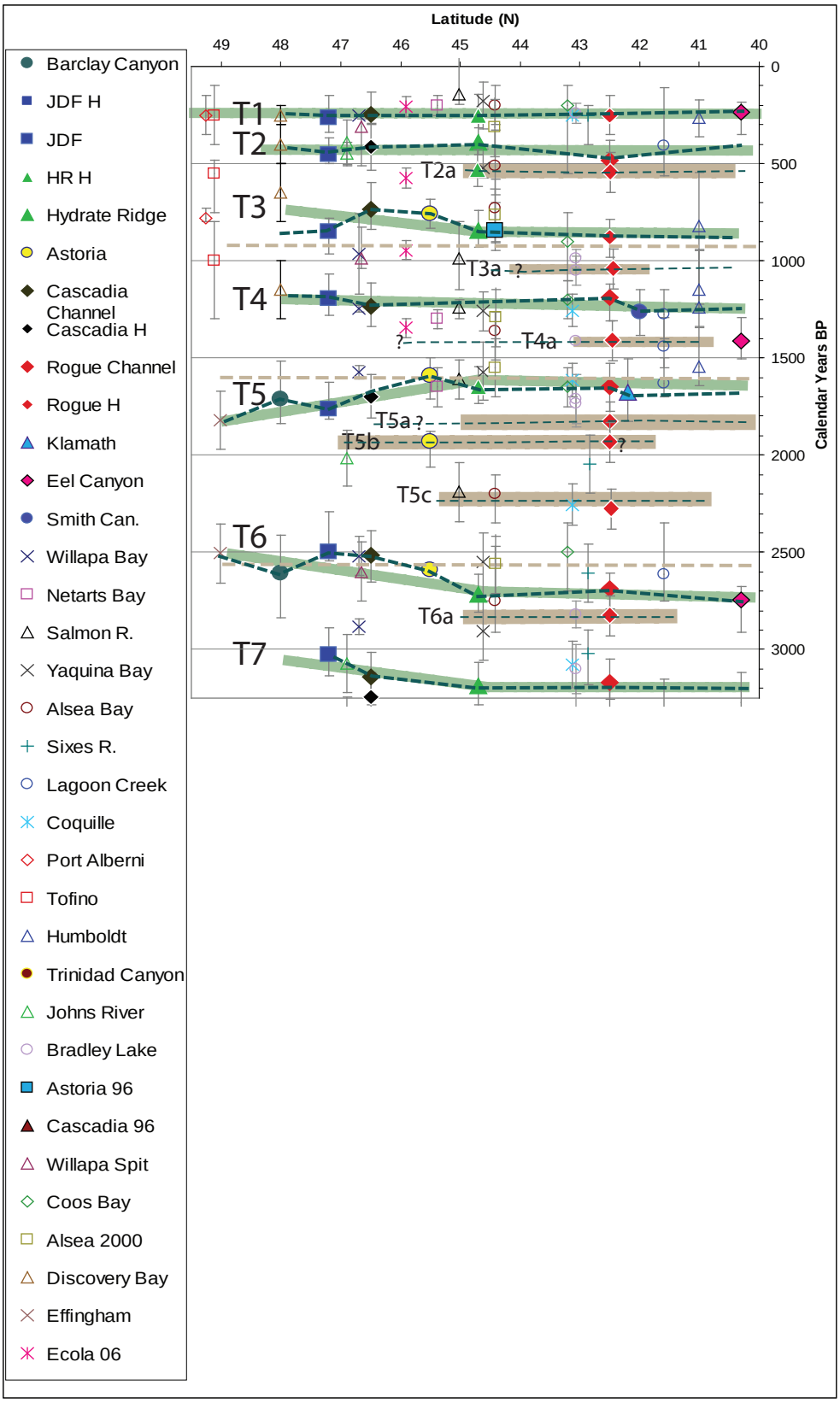

Figure 5. Space time diagram for the Cascadia margin showing land and marine data for the past ~ 3300 years. Filled symbols are marine turbidite data, open symbols are land paleoseismic data. Blue dashed lines show stratigraphic correlation of the turbidite data. Smaller southern Cascadia event use thinner lines. Site localties shown by symbology, locations shown on Figure 1. Marine symbols surrounded by white border are ages calculated from events above , below, or both using hemipelagic thickness and sed. rates. Green (marine) and brown (land) bars are best fitting trends for Cascadia earthquakes. Marine trends show space and time variant trends in some locations and time ranges due to reservoir age variability, further discussed in text. Brown dashed lines show bet fit land-marine age after applying marine prototype reservoir correction.

between offshore and onshore events in time is also striking. We suggest that the smaller events recorded offshore, are in some cases the same events recorded onshore, though we cannot with certainty demonstrate this link. Some of the smallest events offshore likewise are represented by a spotty or absent record onshore. While this reduces our confidence in these events, it is also consistent with smaller earthquakes leaving a more discontinuous geologic record. We also note that the smaller turbidites offshore correspond reasonably well to the local southern Oregon events where they have been dated. In some cases, these turbidites cannot be dated directly, but have hemipelagic ages similar to onshore eathquakes, and lie in time ranges constrained by bracketing turbidite ages that also have corresponding onshore earthquakes. These earthquakes have limited rupture length in both onshore and offshore records, suggesting a first order compatibility between offshore turbidite size, shaking intensity or duration (controlling turbidite volume) and rupture length. The offshore rupture limits reflected in the **Figure 3** correlation are derived from our interpretation of the combined land/marine data shown in **Figure 5**.

Offshore, the turbidite record gives a positive stratigraphic method of determining rupture length, limited by the uncertainty in triggering distance between canyons (estimated to be less than 90- km for full margin events, and almost certainly less for smaller events, Goldfinger et al., 2007a) and uncertainties in correlation. ^{14}C ages for offshore events also provide constraints on rupture lengths. Onshore, the constraints are weaker because individual events cannot be correlated directly. The links between onshore events are thus mostly based on ^{14}C with some additional constraints from the stratigraphic sequences at the land sites. In no cases do we find land events extending beyond the latitude limits of the marine record. In most cases latitude limits are similar, but a few cases, such as T2, the marine correlatives extend to greater latitude limits. Several of the smaller events in the marine record apparently have no land equivalents (T2a and T6a). These are the smallest of the marine events, with narrow latitude limits, thus we suggest that the marine record is likely more sensitive to these small events. Limited rupture lengths and presumably magnitudes for these events may lack sufficient stress drop to generate significant tsunami or land subsidence, though they apparently do generate small correlatable marine turbidites. Alternatively, these small offshore events may not correlate as we infer, and would then be uncorrelated local events of no significance in the marine earthquake record. Although the correlation evidence and limited ^{14}C ages for these events make them less robust than the larger events, their appearance at the same intervals in numerous cores from isolated environments in Cascadia basin channels and slope basin cores makes such a coincidence unlikely.

Cascadia Rupture Modes.

From the combined land/marine stratigraphic and radiocarbon data, we infer that contrast to the northern margin, the southern Cascadia margin records a total of 38 probable earthquakes (10,000 year record, Goldfinger et al., 2006a) that are correlated between multiple sites, and thus define a mean recurrence interval for the southern Cascadia margin of ~260 years in the Holocene. The combined stratigraphic correlations, hemipelagic analysis, and ^{14}C framework represented in the correlation figures, the space time-diagram, and the supplementary tables can be summarized in **Figure 6**, which shows groupings of rupture lengths supported by the combined onshore and offshore records. We show the most recent 3000 year period relevant to

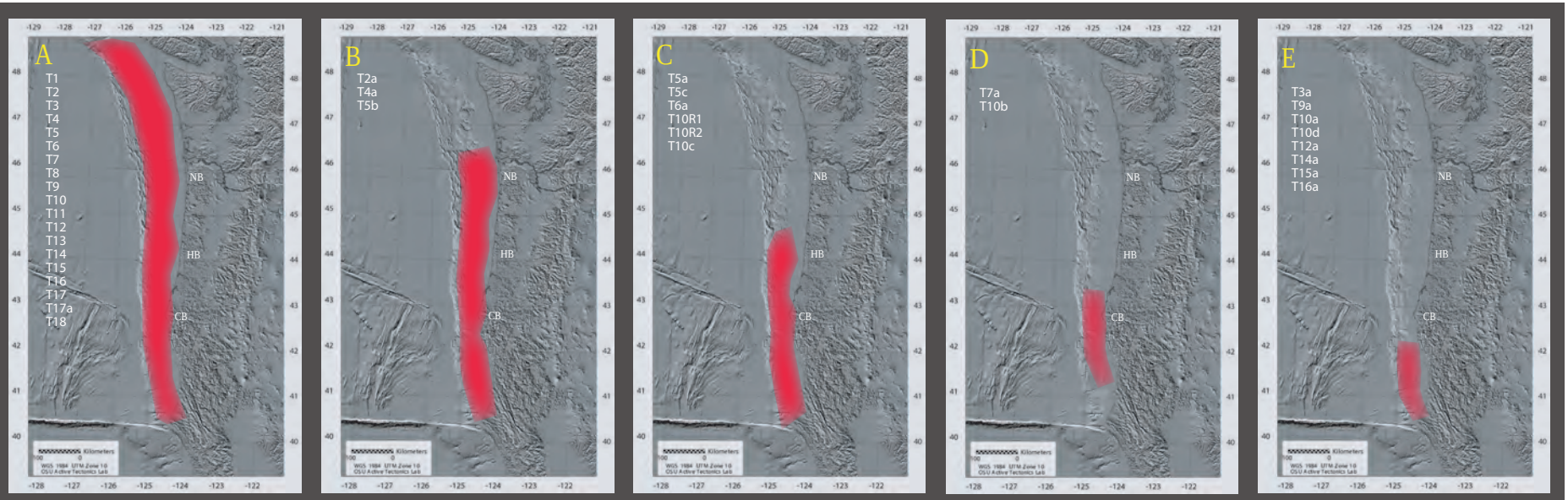

Total 38 events avg recurrence = minimum recurrence 258 years for some southern Cascadia localities

Figure 6 Holocene rupture lengths of Cascadia great earthquakes. Five panels showing Holocene preliminary rupture modes identified using turbidite correlation. A. Full rupture, represented at all sites by 19 events. B. Mid-Southern rupture, Represented at all sites as far south as 41N by three events. C. Southern rupture from central Oregon southward, represented at all sites as far north as 44.5N by four events. D. Southern Oregon events, represented by two events. E. Northern California events, represented by eight events with slightly varying limits shown the same here. See Table 1 for listing of northern and southern limits. Approximate updip and downdip limits from Goldfinger et al., 1992; 1996, 2007c, and Oleskevich et al., 1999.

this paper, the complete Holocene analyses are given in Goldfinger et al., (2008). Overall, the Holocene record suggests that the Cascadia margin effectively has five rupture modes (refined from the four shown in Goldfinger et al., 2006b): 19 full or nearly full -length ruptures (50%); 2 ruptures comprising the central and southern half of the margin (5%), and 17 smaller southern margin ruptures that have three general groupings of rupture length (45%) during the Holocene.

Cascadia-NSAF Temporal Comparison.

The average recurrence interval for the southern Cascadia margin in the last ~ 3000 years is (ignoring the slightly different southern rupture limits) is 3154 (average age of T7) -250)/13 = 223 years. The similarity between the mean NSAF recurrence time and the southern Cascadia recurrence (~200 offshore, 230 onshore vs. ~223 years respectively) and the relatively close correspondence between the AD 1700 Cascadia event and the penultimate NSAF event, at ~ 1700-1760 AD, prompted us to examine both the temporal connection between the two fault systems, and the potential stress interactions between them. In **Figure 7** we plot the NSAF time series over the past ~3000 years with Cascadia events shown using both peak probability and PDF functions for offshore turbidite ages and onshore paleoseismic data. For land ages, we use the combined land-marine dataset to determine the best ages to use for this study based on their reported error ranges, the fit of the reported age to the larger dataset, and the fit of the age within the data reported by the original authors for land data.

In addition to the close correspondence between the Cascadia AD 1700 earthquake, and the penultimate NSAF event ~ 1700-1760 and recurrence intervals noted above, we also see an apparent coincidence of Cascadia events and NSAF events occurring at approximately the same time for 12 and possibly 14 of 15 NSAF earthquakes (**Figure 7**; Goldfinger et al 2007a). During the 0-3000 year period, the combined onshore/offshore paleoseismic record for Cascadia includes 12 events, and two possible additional events.

To a first order, the recurrence intervals for southern NSAF and Cascadia (200 vs. 220) are quite similar, and clearly distinct from northern Cascadia (496-526 years; Goldfinger et al., 2006b; 2007b). If we include the two suspect events described above, the average repeat time for southern Cascadia would be 212 years. For the 15 NSAF events, we observe that with the exceptions of NSAF event T12 (and the weaker associations of T12a and T1) the remaining NSAF earthquakes each have a corresponding Cascadia event in temporal proximity. The relationship can be seen graphically in **Figure 7**.

We can examine the temporal relationship (if any) between the NSAF and southern Cascadia by several methods: the relationship of mean ages, peak probability ages, and probability distributions. These are fully discussed in Goldfinger et al. (2008).

Comparing raw means, for 12 events for which we can make a comparison, the Cascadia turbidite events preceded the NSAF event by an average 37 years (std. dev. 32 years). Considering the time interval by which NSAF events preceded Cascadia, the mean delta would be 150 years, larger by a factor ~ 4. For events interpreted to be the same events onshore (excepting Cascadia T2a and T6a which are not reported), 9 of 12 Cascadia peak ages precede NSAF events, with three ages nearly identical, yielding an average delta of 37 years(std. dev. 42 years) The alternate hypothesis of NSAF precedence yields a mean delta of 202 years, greater by a factor of ~5

If we apply a prototype reservoir model developed during this project to our marine ages, we find that in addition to tighter groupings of land-marine ages which would be expected, the mean delta between the NSAF and preceding Cascadia earthquakes is reduced to 16 years. For Cascadia following the NSAF, the delta is 187 years, larger by a factor of >12. Application of this prototype reservoir age mapping is not included in **Figure 7**, however its application appears promising and is included in Goldfinger et al. (2008) for comparison.

The age series in total suggest a temporal relationship between Cascadia and NSAF events that does not appear to be random, and strongly favors Cascadia earthquakes preceding the NSAF The alternate relationship that Cascadia events consistently post-date NSAF events is possible as well, though the average time separation would be greater by a factor of 4-6. We also note that the Cascadia ages for offshore events may change somewhat as a result of better definition of the marine reservoir correction in the future, and this may help close the gap for some time and latitude ranges for which the modern correction appears to be inadequate.

Coseismic and Postseismic Deformation from Cascadia Earthquakes

In order to quantify the influence of Cascadia earthquakes on the NSAF, we worked with Rolland Burgmann and his PhD student Kelly Grijalva at Cal Berkely to model the coseismic and postseismic deformation from the Cascadia earthquakes. First we verified the geometry of the NSAF system, which has only been poorly mapped previously. Offshore, the NSAF traverses the continental shelf between Point Arena and Point Delgada, and was mapped using early seismic reflection profiles (Curray and Nason, 1967). In 2004 we collected multibeam bathymetric data and several 3.5 kHz profiles across the offshore NSAF. We used these data and a newly released dataset of migrated industry multichannel reflection profiles to verify that the NSAF indeed traverses the shelf and comes ashore again at Point Delgada and verify the original mapping of Curray and Nason. We also observe some additional compressional deformation, particularly within the NE part of the Viscaino block, but are unable to evaluate this deformation in terms of recency and rates, and thus we do not consider it in the subsequent modeling.

We model the elastic coseismic deformation, deformation from deep afterslip, and 60 years of postseismic deformation resulting from viscoelastic relaxation of elastic stress changes due to the earthquake in the mantle. We initially assume that the entire subduction zone slipped in a megathrust event such as the AD 1700 earthquake (Satake et al., 1996, 2003; Goldfinger et al., 2003a), and also model a smaller southern margin earthquake.

The first-order slip model involves 14 m of slip on each of the 16 planes spanning the 1050-km-long megathrust rupture and 7 m of slip on the 8 deep afterslip planes. The elastic coseismic and postseismic deformation is calculated in a layered spherical geometry using the method of *Pollitz* (1996). The geometry of the megathrust rupture is based on the plate-interface model of *Flueck et al.* (1997) and the elastic structure of the Earth is based on the seismically determined global Earth model PREM (Dziewonski and Anderson, 1981). The modeled earthquake has a magnitude of Mw 9.1 based on the fault geometry, slip values and Earth model. Viscoelastic deformation is calculated on a spherical earth using the method of *Pollitz* (1992). We use the preferred spherically layered Earth model presented by *Pollitz et al.* [2006] for a study of postseismic deformation following the 2004 and 2005 Sumatra megathrust events, which employs a

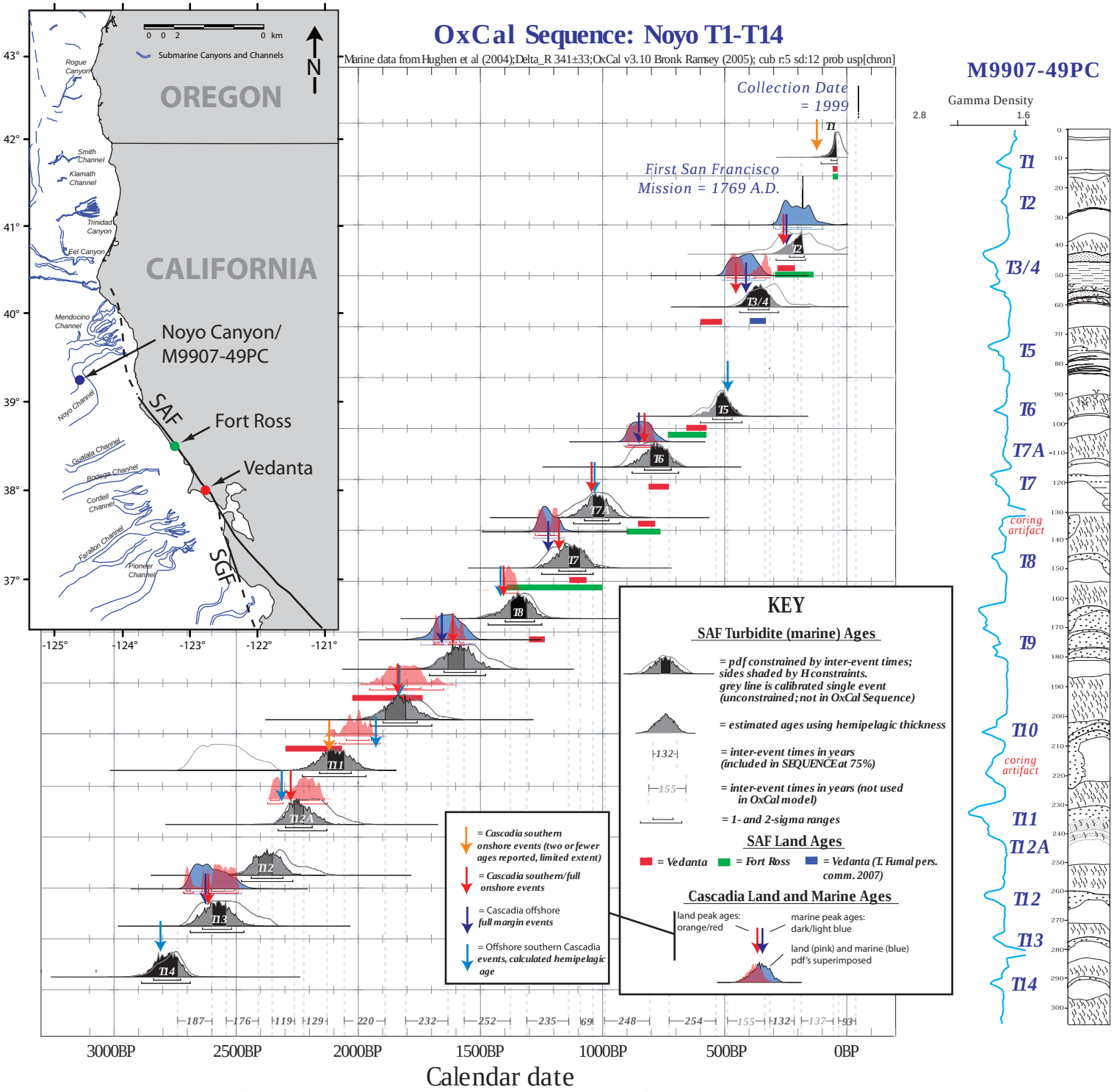

Figure 7. OxCal age model for the youngest 15 events in the NSAF offshore system, and comparison to onshore NSAF ages. Cascadia OxCal PDF's are shown in blue, with lighter blue used where only Hemipelagic ages are available. Land ages from OxCal combines are shown in red. Cascadia mean event ages are also shown with blue arrows for well dated turbidite events, Purple arrows for hemipelagic age estimates, and light red arrows for onshore paleoseismic events. See text for discussion and tables for data used and criteria, and discussion of temporal relationships. Inter-event times based on hemipelagic sediment thickness (represented by gray segments of NSAF PDF's) were used to constrain original 14C calendar age distributions (gray traces) using the SEQUENCE option in OxCal. Inter-event times were estimated by converting hemipelagic sediment thickness between each pair of events to time using the sedimentation rate. Events dated more than once were combined in OxCal prior to calibration if results were in agreement; if not in agreement, the younger radiocarbon age was used in the final model. Five ages are calculated from sedimentation rates where not enough forams were present for 14C dating. The resulting probability distributions (filled black, grey for undated events) are mostly in good agreement with land ages from Fort Ross except for T3-4 and T7a (green lines; Kelson et al., 2006) Vedanta (red lines; Zhang et al., 2006) Bolinas Lagoon and Bodega Bay (Purple lines, Knudsen et al., 2002) and Point Arena (light blue lines, Prentice et al., 2000). Additional Vedanta event is also shown (Fumal pers. comm. 2007) See inset for geographic locations. See Electronic Supplement for OxCal input data and sedimentation rate curves.

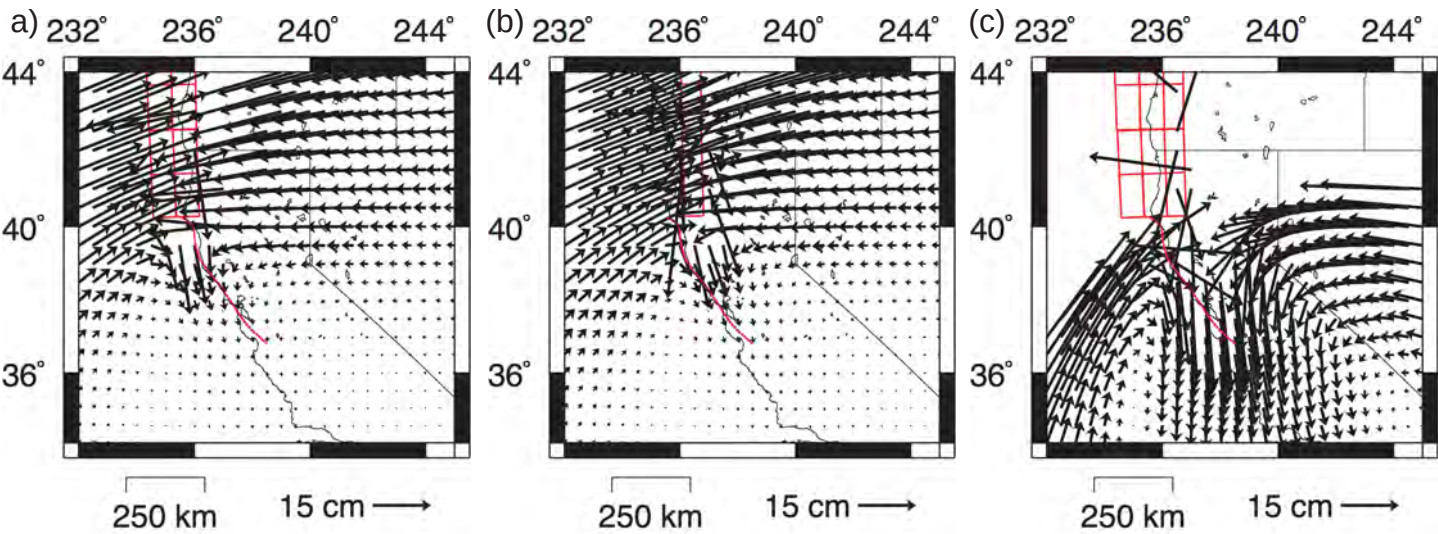

Figure 8. Comparison of the far-field coseismic and postseismic deformation for displacements less than 30 cm at the surface (absent grid points have displacements greater than 30 cm). Total displacement fields in the supplemental materials. A) coseismic deformation from Cascade megathrust B) displacement from afterslip on the Cascade megathrust C) cumulative viscoelastic displacement from Cascade megathrust and afterslip at 1760.

bi-viscous (Burgers body) viscoelastic rheology in the aesthenosphere (Pollitz et al., 2006). In this model the aesthenosphere has an initial short-term viscosity of 5x 10^{17} Pa s that dominates the deformation during the first few years and a long-term viscosity of 1 x 10^{19} Pa s. This model matches both the spatial pattern and temporal evolution of the first year of postseismic GPS measurements in Southeast Asia. The modeled postseismic surface velocities after several decades of transient deformation are also of similar magnitude as those currently measured along the rupture zones of the great 1960 Chile (Hu et al., 2004) and 1964 Alaska (Zweck et al., 2002) earthquakes.

Figure 8 A, B, and C show the far-reaching surface displacement fields (only displacements < 0.3 m are shown) from the coseismic and postseismic deformation models. The horizontal coseismic displacements peak at about 18 m where the megathrust changes strike offshore of Washington**, and** are about 2 cm in the San Francisco Bay Area (**Figure 8A**). Coseismic displacements exceeding 0.1 m extend for up to 500 km to the east and west of the rupture. The horizontal surface displacements resulting from deep afterslip peak at about 2.5 m and are between 2-3 cm in the Bay Area (**Figure 8C**). The cumulative motions from mantle relaxation in the first 60 years of postseismic relaxation exceed 0.1 m to distances greater than 1000 km. The horizontal viscoelastic displacements at the surface peak at about 165 cm and are between 15-25 cm in the Bay Area (**Figure 8B**). However, except for the segment offshore from Pt. Delgada, the NSAF is located in a low–strain lobe for both the coseismic and postseismic deformation.

<u>Stress Changes From Cascadia Earthquakes Along the NSAF</u>

We evaluate the stress changes along the NSAF associated with coseismic and postseismic deformation from Cascadia megathrust events in order to test the possibility that the Cascadia earthquake triggered subsequent NSAF events. We model the Coulomb failure stress (CFS), which takes into consideration both shear- and normal-stress changes across the NSAF. Previous studies have shown that CFS increases of 1-3 bars are generally sufficient to trigger seismicity (e.g., Stein & Lisowski 1983, Toda et al. 1998, Rydelek and Sacks, 1999, Freed, 2005). We use a CFS function given by CFS = $\Delta t + \mu' \Delta\sigma_n$, which defines CFS as a sum of the change in shear stress τ and the change in normal stress σ_n, multiplied by an effective coefficient of friction. Positive CFS enhances loading on the right-lateral NSAF. CFS is modeled on 48 NSAF receiver fault segments at 10 km depth, based on the geometry of the 1906 earthquake rupture (Thatcher et al., 1997), assuming $\mu' = 0.4$. CFS values are also computed for a ~100-km wide zone along the NSAF, assuming the same receiver-fault geometry.

Stress changes along the NSAF due to a Cascadia megathrust rupture and subsequent relaxation vary significantly along the fault due to both changes in distance and strike of the fault, ranging from N55W to N1W. Overall, we find that coseismic CFS changes are large and likely to enhance subsequent rupture only on the northernmost segment of the NSAF (**Figure 9A**). CFS changes along the remainder of the fault are modest as the NSAF lies in a nodal lobe of coseismic deformation. Postseismic viscous relaxation appears to reduce CFS along much of the NSAF and can therefore not be considered as a significant triggering mechanism in this case. Future work will evaluate if consideration of three-dimensional heterogeneity of Earth rheology significantly changes this conclusion.

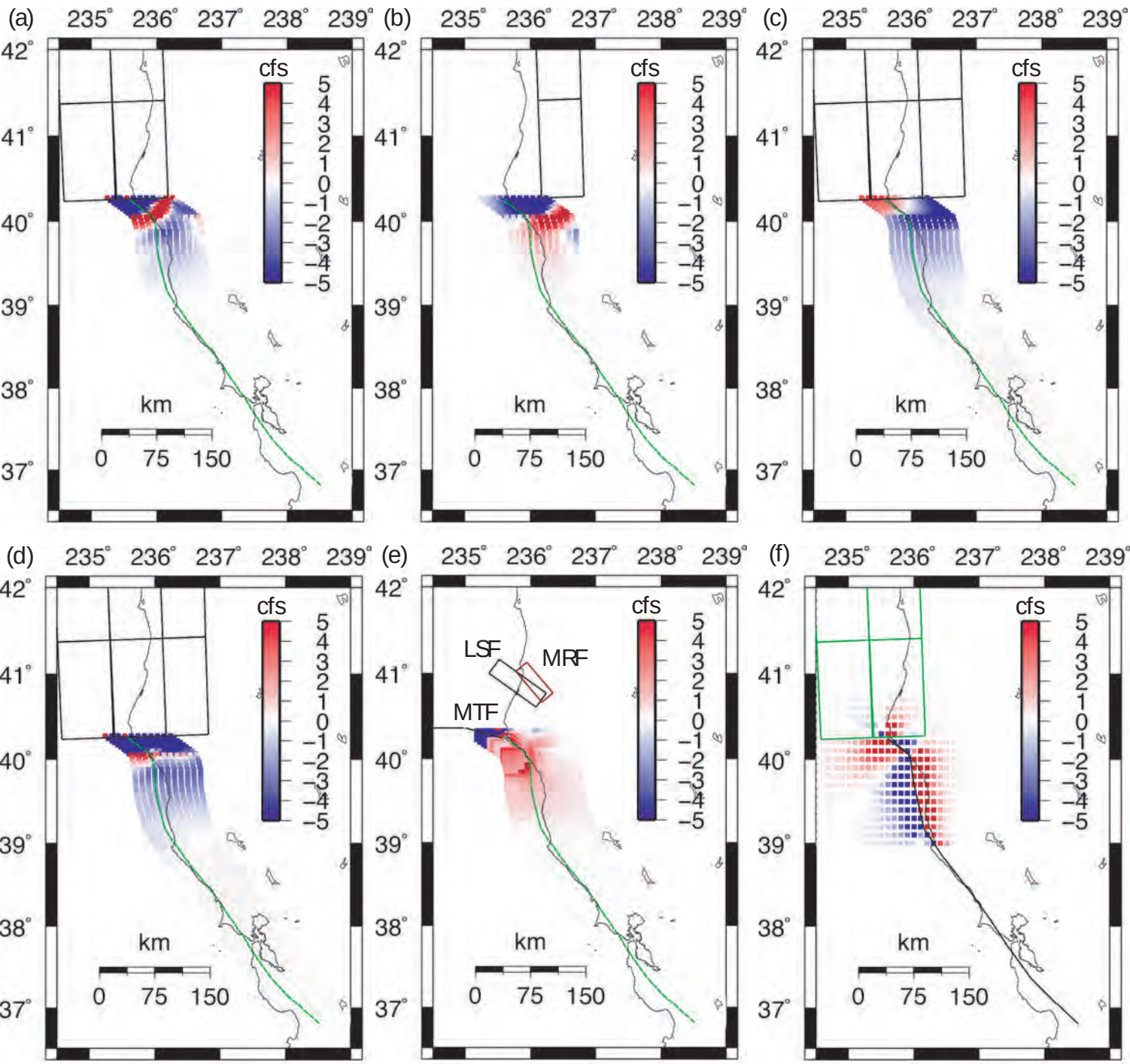

Figure 9. a) Comparison of CFS changes (bars) on the NSAF from A) coseismic deformation B) afterslip C) viscoelastic relaxation D) combined coseismic, afterslip, and viscoelastic relaxation E) coseismic deformation and viscoelastic relaxation from Mendocino Transform Fault (MTF) and Little Salmon Fault (LSF). Fault segments in black are source faults, green segments signify receiver faults. F) CFS change on the Cascadia receiver faults from a NSAF earthquake.

The coseismic deformation increased CFS at 10 km depth by a maximum of about 9 bars in the section of the fault near Point Delgada (**Figure 8A**). The CFS resulting from the viscous deformation peaks at about 2.5 bars; however, this peak is in the northernmost region of the fault where there is a large negative coseismic CFS (**Figure 8C**). Postseismic afterslip both increases and reduces CFS along the NSAF, but its negative peak reduces the extent of the largest positive coseismic CFS by half (**Figure 8B**). We compare our uniform-slip full-margin earthquake model with coseismic and postseimic CFS changes resulting from a southern Cascadia earthquake, with 8 m of slip on the six southernmost Cascade fault planes (380 km strike length) and from a heterogeneous full-margin earthquake that includes less slip on the southern fault planes (Pollitz et al., 2007). Total CFS on the NSAF from both the southern Cascadia earthquake and the heterogeneous full-margin earthquake peaks in the same northern location as from the homogenous full margin model, however the CFS peaks are reduced by about a factor of two. Based on these results, it appears that the most likely nucleation point of a triggered NSAF event, from whichever of the three Cascadia source models, would be near Point Delgada. The coseismic CFS alone would be large enough to trigger an earthquake, while the postseismic contributions from the viscous relaxation and afterslip do not significantly increase the total CFS on the NSAF.

We also tested the reverse triggering scenario and modeled CFS on the Cascadia receiver planes from a NSAF type earthquake using a distributed slip model for the 1906 earthquake (Thatcher et al., 1997.) The maximum positive coseismic CFS on the southern tip of the margin is about 20 bars at depths between 12-16 km (**Figure 12F**). At these depths, CFS increases of at least 1 bar extend north for about 30-40 km. The CFS resulting from viscoelastic relaxation is mostly negative on the southern Cascade receiver planes. This may be sufficient to trigger an earthquake on southern Cascadia or on the smaller upper plate thrust faults, such as the MRF and the LSF, although the 1906 events failed to do so. The paleoseismic record however strongly favors the former case, with Cascadia events preceding the NSAF by ~ 50 years, whereas Cascadia earthquakes follow NSAF events on average by 150 years.

Further discussion of these fault relationships can be found in Goldfinger et al. (2008).

Publications from this grant:

Nelson, C. H., Goldfinger, C. Johnson, J.E., Dunhill, G, 2000, Variation of Modern Turbidite Systems Along the Subduction Zone Margin of Cascadia Basin and Implications for Turbidite Reservoir Beds, *in* Weimer, P.W., Nelson, C. H. et al. (eds.), Deep-water Reservoirs of the World, Gulf Coast Section Society of Economic Paleontologists and Mineralogists Foundation 20th Annual Research Conference, Dec.3, 2000, Houston, TX., 31p, 15 Figures.

Goldfinger, C., C.H. Nelson, J.E. Johnson, M.A. Arsenault, A. Eriksson, E. Karabanov, and J. Chaytor, (2004b). Physical Property Correlations from Cascadia Great Earthquakes: What Are They Telling Us About The Triggering Events? Eos Trans. AGU, v. 85 (47), Fall Meeting Supl. Abstract OS21E-01.

Goldfinger, C., A. Morey, and C.H. Nelson (2006a). Deep-Water Turbidites as Holocene Earthquake Proxies along the Northern San Andreas Fault System, *Seismological Research Letters* **77**(2), 195-196.

Goldfinger, C., A. Morey, M. Erhardt, C.H. Nelson, J. Gutierrez-Pastor, R. Enkin, and A. Dallimore (2006b). Cascadia Great Earthquake Recurrence: Rupture Lengths, Correlations and Constrained OxCal Analysis of Event Ages, proceedings of the USGS Tsunami Sources Workshop, Diggles, Geist, and Lee, eds. CD-ROM, April 21 and 22, 2006.

Goldfinger, C., A.E. Morey, C.H. Nelson, J. Gutierrez-Pastor, J.E. Johnson, E. Karabanov, J. Chaytor, and A. Ericsson (2007a). Rupture Lengths and Temporal History of Significant Earthquakes on the Offshore and North Coast Segments of the Northern San Andreas Fault Based on Turbidite Stratigraphy, *Earth and Planetary Science Letters* **254**, 9-27.

Goldfinger, C., and C.H. Nelson (2007b). Holocene Recurrence of Cascadia Great Earthquakes based on the Turbidite Event Record, *Nature*, in revision.

Goldfinger, C., 2007c, Paleoseismic Slip History and Geologic Constraints on Splay Faulting and Interplate Coupling along the Cascadia Subduction Zone: DOGAMI Final Project Report 07-02 Corvallis, Oregon State University, 13 pp.

Goldfinger, C., C.H. Nelson, A.E. Morey, J. Gutierrez-Pastor, J.E. Johnson, E. Karabanov, J. Chaytor, G. Dunhill, and A. Ericsson (2008). Rupture Lengths and Temporal History of Cascadia Great Earthquakes Based on Turbidite Stratigraphy, USGS professional Paper 1661-F, *in* Kayen, R. ed, Earthquake hazards of the Pacific Northwest Coastal and Marine regions. 192 p. In prep.

Goldfinger, C. Nelson, C. H., Johnson, J., 2003, Holocene Earthquake Records From the Cascadia Subduction Zone and Northern San Andreas Fault Based on Precise Dating of Offshore Turbidites Annual Reviews of Earth and Planetary Sciences, v. 31, p. 555-577.

Goldfinger, C. Nelson, C. H., Johnson, J., 2003, in press, Deep-Water Turbidites as Holocene Earthquake Proxies: The Cascadia Subduction Zone and Northern San Andreas Fault Systems. *In*, Pantosti, D. Berryman, K., eds., Annali Geofisica Special issue on Paleoseismology.

Gutierrez-Pastor, J., Hans Nelson, H.C., Goldfinger, C., Carlota Escutia, A. and Morey, A., Earthquake control and frequency of generation on the Cascadia and San Andreas active continental margins, SEPM Special Paper on turbidites, in press 2007.

Goldfinger, C., Grijalva, K., Burgmann, R., Morey, A., Johnson, J.E., Nelson, C.H., Gutiérrez-Pastor, J., Karabanov, E., Gracia, E., in review, 2008, Late Holocene Rupture of the Northern San Andreas Fault and Possible Stress Linkage to the

Cascadia Subduction Zone, Bulletin if the Seismological Society of America Special Volume on the 1906 earthquake

11 additional abstracts from GSA, AGU, AAPG and other meetings.

Non-Technical Summary

Past Great Earthquakes along the Cascadia margin have left a record of submarine landslides spanning more than 10,000 years. Dating of these events has shown that the average repeat time is ~ 500 yearsalong the northern margin, 260 years in the south. A variety of tests of event timing shows that 19 times in the last 10,000 years, at least 700 km of the Cascadia margin has ruptured simultaneously. Cascadia earthquakes may trigger earthquakes along the Northern San Andreas Fault.